Raman spectroscopy of oxygen carrier particles in harsh environments

John Kirtley[a], Victoria Leichner[a], and Hergen Eilers*[a]
[a]Applied Sciences Laboratory, Institute for Shock Physics, Washington State University, Spokane, WA, USA 99202

ABSTRACT

Fossil fuel combustion processes generate CO_2, a greenhouse gas of considerable concern. To reduce this emission, the National Energy Technology Laboratory (NETL) is evaluating alternative combustion approaches, including chemical looping combustion (CLC). This technique generates relatively pure CO_2, suitable for subsequent capture and storage. CLC uses oxygen-carrier particles (OCPs) such as iron oxides, copper oxides, calcium sulfates, etc. to provide oxygen for the combustion process. Optimization of the overall combustion process requires knowledge of the oxidation state (e.g., content of Fe_2O_3 vs. Fe_3O_4) of the OCPs during the different stages of the CLC process. Unfortunately, the ability to make on-line measurements of the oxidation state of OCPs in harsh environments is lacking and new sensors need to be developed.

We are evaluating non-contact, stand-off Raman spectroscopy to determine the relative concentrations of the oxidized and reduced forms of OCPs at temperatures between 800 °C and 1000 °C, and pressures of about 10 atm. Using cw and pulsed Raman spectroscopy, in combination with a pressurized high-temperature sample chamber, we have optimized the operating parameters such as laser wavelength, laser intensity, collection optic design, focal spot size, etc. and measured Raman spectra of various OCP materials at high temperatures. To extract from the Raman spectra relevant information such as the concentration ratio of a material in different oxidation states, the measured data needs to be processed, and statistical modeling and multivariate calibration need to be performed.

Keywords: Fossil-fuel combustion, CO_2 emission, closed-loop combustion, process control, oxidation state monitoring, harsh environments, Raman spectroscopy

1. INTRODUCTION

The need for cleaner energy systems, including CO_2 capture technologies, is driving the current development of new technologies such as chemical looping combustion (CLC) and chemical looping gasification (CLG). Specific processes that are under development for using solid fossil fuels are in-situ Gasification Chemical-Looping Combustion (iG-CLC) and Chemical Looping with Oxygen Uncoupling (CLOU). Many authors, including Wang et al., Luo et al., and Moghtaderi have described the development of these various processes in some excellent review articles.[1-3]

Chemical looping is based on using oxygen carriers (e.g., iron oxides, copper oxides, calcium sulfates, etc.) to repeatedly provide the oxygen for the fuel combustion. While many different technology variations are being investigated, the typical process uses two reactors, a fuel reactor and an air reactor. In the fuel reactor, fuel reacts with oxygen released from OCPs, generating energy, reduced OCPs, and H_2O and CO_2 as waste products. In the air reactor, the reduced OCPs react with the oxygen in air and are oxidized for further use in the fuel reactor.

To optimize the overall process performance, it is critical that the properties of the OCPs are well-defined and maintained for their specific purpose during the different stages of the CLC process. One of the critical properties of the OCPs is their oxidation state (e.g., content of Fe_2O_3 vs. Fe_3O_4) as it affects the fundamental operation of the CLC process. Unfortunately, the ability to make on-line measurements of the oxidation state of OCPs is lacking and new sensors need to be developed.

*eilers@wsu.edu; phone 1-509-358-7681; fax 1-509-358-7721 www.asl.wsu.edu

NETL is interested in developing and demonstrating methods to conduct online measurements of OCPs as they move past specific locations within advanced energy systems. There are several challenges associated with these methods, including: (i) capable of identifying different oxidation states (e.g., Fe_2O_3 vs. Fe_3O_4); (ii) in-situ (on-line) approach that does not interrupt the process flow; (iii) stand-off method to avoid handling high-temperature materials at elevated pressures; (iv) fast-enough for in-situ measurements; (v) fast analysis to provide immediate feedback; (vi) capable of handling various sample geometries; etc. These constraints rule out chemical methods such as iodometry. Also, x-ray-based or electron-beam based techniques such as XPX, XANES, EELS, etc., besides being expensive, would be very difficult to implement.

However, one approach that has been evaluated for similar circumstances, is high-temperature Raman spectroscopy. Li et al. studied the feasibility of this approach for on-line monitoring and product control of glass vitrification.[4] These authors concluded that high-temperature Raman spectroscopy in combination with statistical models, is a feasible approach for on-line process control. Using the initial findings by Li et al., we have started to develop high-temperature Raman spectroscopy for the measurement of the oxidation state of OCPs.

2. METHODOLOGY

2.1 Oxygen carrier particles

Specific OCPs and their relevant properties have been investigated by many different researchers.[1, 3-27] In general, desired properties include: high conversion efficiency, high reactivity with the fuel, long lifetime, low agglomeration, and low cost and environmental impact.[28] Typically, a specific type of OCP works best for a specific CLC technique. The reactions for the OCPs occurring in the two reactors can be summarized as:[3]

$$\text{Fuel} + n\text{Me}_x\text{O}_y \rightarrow n\text{MexO}_{y-1} + \text{H}_2\text{O} + \text{CO}_2 \quad (1)$$

$$\text{Me}_x\text{O}_{y-1} + \tfrac{1}{2}\,\text{O}_2 \rightarrow \text{Me}_x\text{O}_y \quad (2)$$

Some of the most promising OCPs include iron oxide, copper oxide, and calcium sulfate, as well as certain mixtures of these materials. More detailed information about OCPs can be found in the listed references.

The samples studied in this work include calcium sulfate (Sigma Aldrich, -325 mesh), fine-powdered hematite (α-Fe_2O_3, Sigma Aldrich, <5 μm), coarse hematite (Alfa Aesar, 3-12 mm), and magnetite (Fe_3O_4, Sigma-Aldrich, 3 μm - 70 μm). Generally, Raman measurements were collected from loose powders. Where mentioned in the text, however, measurements were also collected from a pressed, high-density form of the 5 μm hematite powder. In addition, the coarse hematite was prepared by grinding with a mortar and pestle, followed by sieving to achieve the desired particle size distribution.

2.2 Raman spectroscopy

Raman spectroscopy is a well-known optical analysis technique that relies on the Raman effect discovered by C. V. Raman and K. S. Krishnan in 1928. The nature of the Raman effect, implementations and applications of Raman spectroscopy, and its many advantages have been described in many books and review articles.[29-40] The following is a brief summary of the most important aspects as they relate to our work, and it is based on the listed references.

Raman spectroscopy typically focuses on identifying vibrational transitions (although other types of transitions such as rotational can also be measured) that are unique to molecules and extended solids, providing a "molecular fingerprint." Unlike infrared (IR) spectroscopy in which the observed vibrational transitions depend on changes in the electric dipole moment, transitions observed in Raman spectroscopy depend on changes in the polarizability of a molecule. Raman scattering refers to the observation of inelastically-scattered light during the interaction of light with a molecule. While the vast majority of light is scattered elastically (i.e., the scattered light has the same wavelength as the incoming light, also called Rayleigh scattering), a small fraction (about 1 in 10^7) of the incoming light is scattered at different wavelengths. Also, scattering depends strongly on the wavelength of light as $\left(\frac{1}{\lambda}\right)^4$.

Scattering can be described as the excitation and de-excitation of a virtual state. In Rayleigh (elastic) scattering, the initial and final states are identical. If the final state corresponds to a higher (lower) excited vibrational state than the initial vibrational state, it is called Stokes (anti-Stokes) scattering, see Figure 1. The difference in wavelength between incoming and scattered light corresponds to the energy of a vibrational transition. The probability for anti-Stokes scattering depends

on the energetic difference between the initial and final vibrational states and the temperature, as both of these parameters determine the population of the higher-lying vibrational state. As temperature increases, the population of higher-energy vibrational states increases, thereby increasing the anti-Stokes signal intensity. By simultaneously measuring the anti-Stokes and Stokes scattering intensities, it is also possible to determine the temperature of the material under investigation.

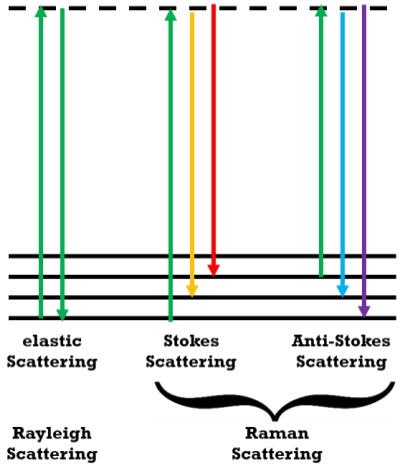

Figure 1. Rayleigh and Raman scattering.

Raman spectroscopy has been widely used to study crystalline and amorphous materials at high temperatures and at high pressures. For example, Garces et al. studied the high temperature interactions of yttria-stabilized zirconia and calcium-magnesium-alumino-silicate at temperatures up to 800 °C,[41] while Le Parc et al. studied the structure of SiO_2-GeO_2 glasses of different compositions at temperatures up to 1100 °C.[42] Mysen and Frantz studied the BaO-SiO_2 system at temperatures as high as 1669 °C.[43] Simultaneous high-temperature and high-pressure Raman measurements have been reported for YBO_3:Eu^{3+}, Mg_2SiO_4, $CaGeO_3$, $CaBSiO_4(OH)$, and many other systems.[44-47] Also, in-situ in-line monitoring using Raman spectroscopy has been reported for pharmaceutical crystallization and solids elaboration processes.[32] Finally, Raman spectroscopy has also been used for high-temperature on-line monitoring of glass melts.[34] In addition, statistical models have been developed for the analysis of high-temperature on-line monitoring of glass melts.[48] Taken together, these earlier reports indicate that high-temperature Raman spectroscopy is a promising approach for on-line monitoring of the oxidation state of OCPs.

2.3 Sample heating and temperature measurements

For the characterization and evaluation of our approach, we use a custom-designed stainless-steel chamber that allows us to heat OCPs to temperatures above 1000 °C and pressures up to 10 atm. The chamber is typically filled with nitrogen (industrial grade) or argon (Praxair, 99.9999%). The chamber uses a Raman-grade CaF_2 window (CrysTran) which has been designed to have only one Raman peak at 321 cm^{-1}, minimizing interference with Raman signals from other sources. The window is kept sufficiently cool to avoid potential problems due to the very high coefficient of thermal expansion (CTE) of CaF_2. In addition, a mechanical shutter inside the chamber is used to protect the window between measurements. Figure 2 shows the water-cooled chamber with the heated OCPs. The OCPs are located in an alumina-coated tungsten basket (Ted Pella) which is connected to a power supply (AmeTek). The temperature is controlled via a K or N-type thermocouple and a PID controller (Omega).

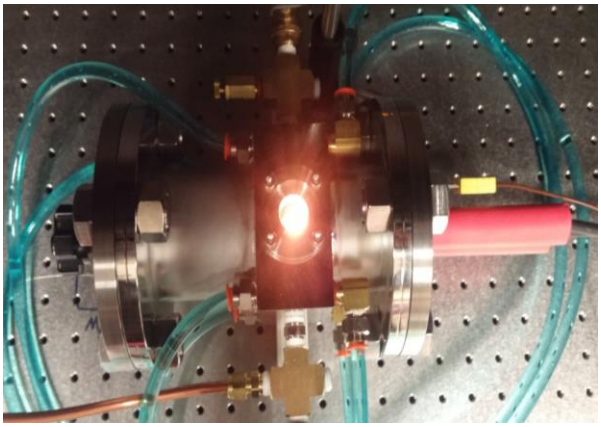

Figure 2. High-temperature sample chamber.

2.4 Instrumentation

A schematic of the envisioned online measurement system is shown in Figure 3. A laser is directed onto the area of interest, and scattered light is collected using a telescope, which guides the light into a spectrometer with attached detector. The signal is constantly monitored by a computer which uses an analysis algorithm to convert the Raman spectra into concentration data.

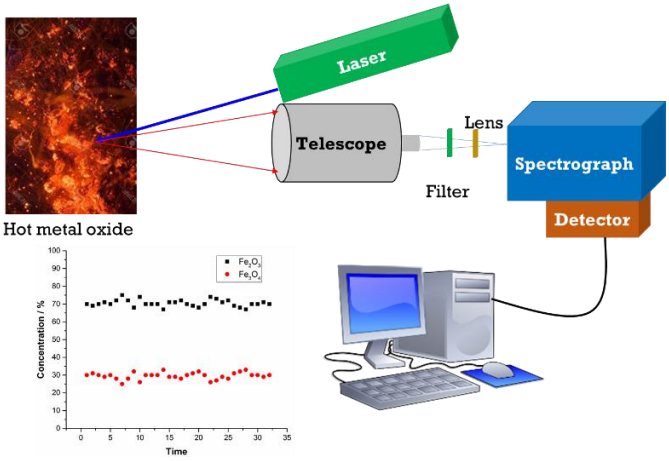

Figure 3. Schematic of the envisioned online measurement system

As mentioned above, the on-line analysis of the oxidation state of OCPs poses some general challenges such as performing this analysis from a stand-off distance, and performing the measurements and analysis fast enough to provide system feedback. These general challenges lead to specific issues when using Raman spectroscopy. The very low probability for Raman scattering to occur (about 1 in 10,000,000 photons impinging on the sample) combined with the loss of directionality of Raman scattered photons, requires efficient collection of scattered light. The experimental parameters for the Raman setup need to be optimized to maximize S/N over the desired data acquisition period. Parameters to consider include: laser wavelength, laser operation mode (i.e., pulsed vs. cw), velocity of OCP movement vs. required acquisition time, distance of OCPs from collection optics, type of collection optics, etc.

Many Raman measurements are conducted using cw near-infrared (NIR) laser sources (e.g., 785 nm). Using a NIR wavelength usually prevents the generation of fluorescence from the sample, significantly improving the S/N. However, since scattering is proportional to $\left(\frac{1}{\lambda}\right)^4$, using an ultraviolet wavelength (e.g., 325 nm) can increase the scattering intensity by more than a factor of 30. While such an increase may be desirable, UV wavelengths tend to result in more fluorescence, which can decrease the S/N. The selection of the right wavelength is often a trade-off between increasing the scattering signal and minimizing fluorescence.

One of the main concerns for performing Raman measurements of samples at high temperature is the presence of strong blackbody radiation. Blackbody radiation (Planck distribution) is strongly dependent on temperature, and the peak intensity shifts to shorter wavelengths as the temperature increases. Comparing blackbody radiation at 785 nm shows that its intensity at 1000 °C is almost 20 orders of magnitude stronger than at 20 °C, while at 325 nm the increase is almost 48 orders of magnitude. Comparing the blackbody radiation intensity at 325 nm and at 785 nm, however, shows that the intensity at the shorter wavelength is more than 6 orders of magnitude less than at the longer wavelength. This comparison makes a strong case for using UV wavelengths for Raman measurements at high temperatures. Li et al. compared the use of cw 325 nm measurements with pulse/time-gated 532 nm measurements for samples at high temperature.[33] These authors were able to measure the high-temperature Raman spectra using either approach. However, differences in the spectra for the two wavelengths are apparent but are difficult to interpret because the temperature control for the UV measurements appeared to be somewhat lacking in their experiments. Nevertheless, the Raman spectra measured using the UV wavelength show a better S/N than those measured using 532 nm.

Several authors have reported on stand-off Raman spectroscopy.[49-52] Hobro and Lendle review various experimental layouts that have been used for a variety of applications including geology, chemical detection, explosives detection, art and archaeology, etc.[53] The majority of these systems use pulsed laser sources operating in the 10 Hz to 30 Hz range using visible and UV wavelengths, and laser pulse powers between 7 mJ and 450 mJ. For example, Gaft and Nagli report on UV gated Raman spectroscopy for the stand-off detection of explosives, while Misra et al. report on pulsed gated Raman spectroscopy for the identification of minerals, and compare several specific approaches.[54, 55] These authors report the best results when using a pulse/time-gated approach.

A schematic of our laboratory-based setup is shown in Figure 4. We use a variety of cw and pulsed laser sources with different wavelengths to evaluate the best operating conditions for our high-temperature measurements. The lasers include a Coherent Verdi V5 cw laser operating at 532 nm, a Quanta-Ray Nd:YAG pulsed laser operating at 10 Hz at 355 nm and 532 nm; and, when coupled with an optical parametric oscillator, 785 nm, a Meredith Instruments Helium-Neon cw laser operating at 633 nm, an Ondax single frequency cw diode laser operating at 785 nm, an Opto Engine solid state cw laser operating at 360 nm, and a Photonics Industries pulsed laser operating at 200 kHz and 355 nm. Within the visible/NIR wavelength region, laser light was focused using a Mitutoyo microscope objective (20x, 10x, 5x with working distances of 20.0 mm, 30.5 mm, and 37.5 mm, respectively). In the UV, laser light was focused using a 40 mm plano-convex lens. The same focusing optic collected the scattered light and guided it through various optical elements, including a notch filter or bandpass filter into an Acton 2500i spectrometer with an 1800 g/mm grating with attached liquid-nitrogen-cooled Spec-10 (PI) detector. For gated measurements, this detector was replaced with a PI Max3 camera. WinSpec (PI) is used for the data acquisition and OriginPro (OriginLab) is used for the analysis.

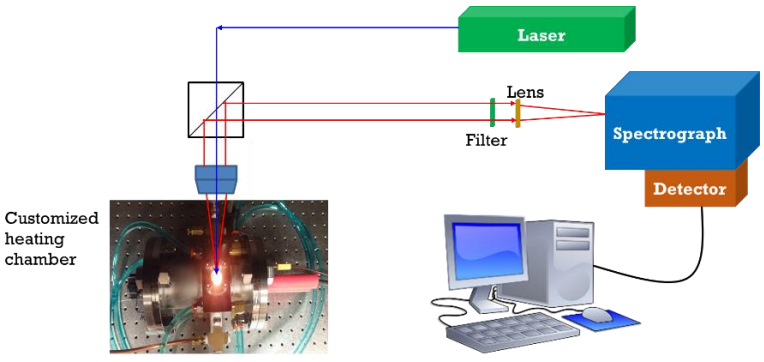

Figure 4. Schematic of our laboratory-based setup.

3. RESULTS

3.1 Calcium sulfate

The initial, envisioned approach used a pulsed laser coupled with time-gated detection to measure Raman spectra from high-temperature OCPs during each pulse while rejecting most radiative background between pulses. For calcium sulfate, an OCP with strong Raman scattering, this approach was successful for temperatures up to 1066 °C, resulting in spectra

with almost no thermal background and clear Raman signal (Figure 5). The temperature-shifted ν_1 mode of anhydrite is clearly visible at 1000 cm^{-1}. However, the signal to noise was limited in part by the light intensity of the laser, which was in turn limited by the appearance of laser-induced breakdown (LIBS) from the sample, accompanied by lower or usually absent Raman signatures. This phenomenon became an increasing problem at higher temperatures. More details from this study are available in a recent publication[56] that includes: 1) a comparison of cw results with pulsed/time gated spectra, 2) an evaluation of experimental parameters influencing LIBS at high temperature, and 3) temperature estimates from the spectra.

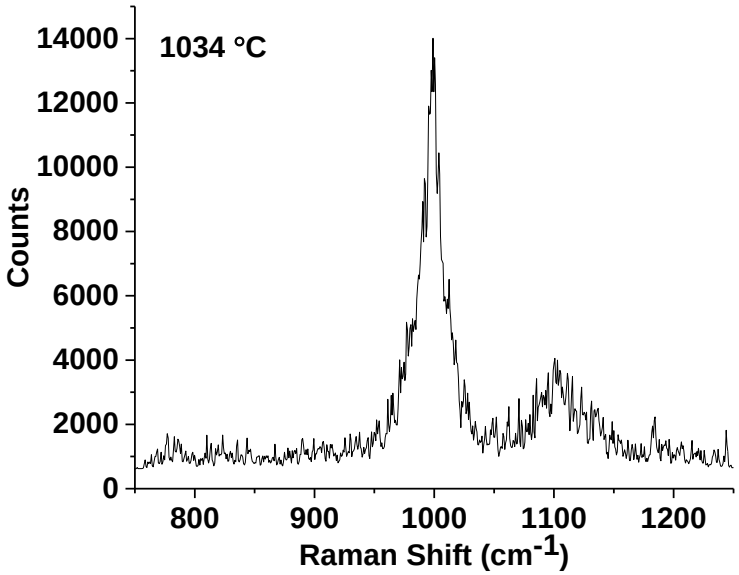

Figure 5. Single-pulse raw Raman spectrum from high-temperature calcium sulfate using the PI Max3 camera. The 0.6 mJ, 532 nm pulse was composed of a pulse train 130 μs long.[56]

3.2 Iron oxide

Iron oxides, specifically hematite and magnetite, because of their availability, low cost, and thermal stability, are advantageous as OCPs over calcium sulfate/sulfite, which can decompose to produce SO_x pollutants. However, in the context of developing a sensor, able to quantitatively discriminate between hematite and magnetite at high temperatures, sufficient Raman S/N must be achieved, and these materials have proven challenging. This is in large part because of their weak Raman cross sections, strong light absorbance, and instability to intense light. The latter two challenges might in principle be overcome by choosing an excitation wavelength in regions in which light absorbance is minimized. In these regions, scattered Raman light should increase, and the likelihood of sample breakdown or heating under intense illumination is reduced. To gain a qualitative understanding of each material's wavelength-dependent absorbance, we measured light scattered from each material in a diffuse reflection integrating sphere, and calculated absorbance (Figure 6). For hematite, lower absorbance is present in the red/near infrared wavelengths while magnetite demonstrates relatively high absorption at all wavelengths, though slightly less in the ultraviolet. This wavelength-dependent property of hematite and magnetite is only one among many factors that influences Raman S/N; as mentioned earlier, thermal background is another influential concern that is strongest in the visible/near-infrared and decreases with wavelength.

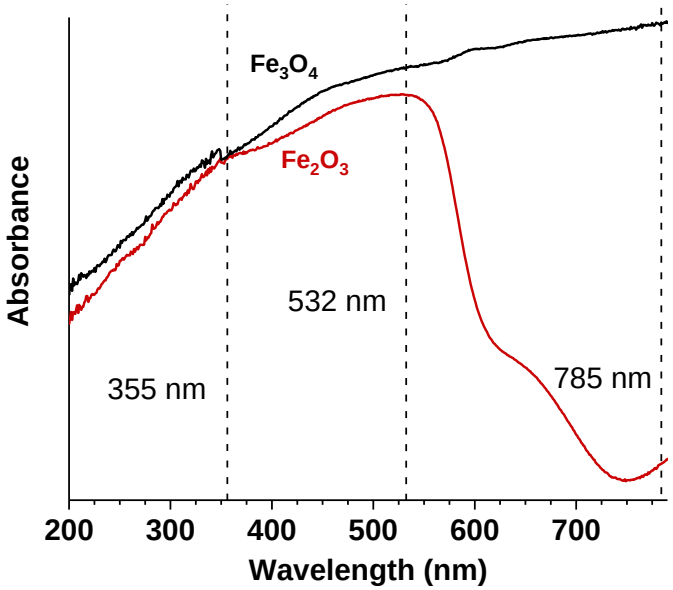

Figure 6. Absorbance spectra from fine-powdered Fe_2O_3 and Fe_3O_4, determined by measuring scattered light within a diffuse reflectance chamber.

Pulsed excitation

The initial, envisioned approach using pulsed-light/time-gating would temporally filter out most of the thermal background from the weak iron oxide Raman signals, as was successfully demonstrated in the calcium sulfate studies. However, this approach also requires that the materials can withstand relatively high light intensities without becoming damaged. Indeed, when we used 10 Hz laser pulses with peak intensities ranging from ~10^9 W/cm^2 to ~10^{12} W/cm^2, our attempts to measure Raman signal from hematite and magnetite were unsuccessful and generally led to sample damage, evidenced by pitting and/or laser-induced breakdown spectra (LIBS). Even at 785 nm, where hematite's light absorbance is weaker we still observe LIBS. Unlike Raman, LIBS cannot readily distinguish between hematite and magnetite.[57]

In contrast with the above results, a 200 kHz, 15 ns, 355 nm laser was more successful. In fact, using this method, Raman spectra from hematite powder were measured to temperatures > 900 °C, using an ungated CCD detector. The key difference using this pulsed laser is that the peak light intensity was much lower than earlier pulsed measurements--on the order of 10^6 W/cm^2, suggesting that relatively low peak powers are required to avoid LIBS and produce Raman signal. In the calcium sulfate studies mentioned above, a threshold intensity was also identified when LIBS appeared, albeit much higher (10^{11} W/cm^2).[56] These results also suggest that low-intensity, quasi-cw lasers at visible wavelengths may successfully measure Raman spectra from high-temperature hematite, especially when coupled with time-gating to remove most thermal background.

CW excitation

The greatest success for measuring Raman signals from iron oxides came by using cw excitation, rather than pulsed, at a variety of wavelengths. This is primarily due to the lower light intensity at the sample—leading to no observed LIBS. In this case, the maximum light intensity was constrained by localized heating—which can lead to high noise backgrounds, and sample phase changes. Table 1 provides a summary of optimized light intensities determined for hematite powders at several wavelengths (with the exception of 360 nm). For room-temperature hematite powders, the strongest Raman signals came from excitation in the red (633 nm) and NIR (785 nm), relative to the green (532 nm), likely due to lower light absorbance. Additionally, at 633 nm, Raman scattering is also aided by resonance enhancement.[58] Unfortunately, these advantages in the red/NIR are lost at higher temperatures, when absorption increases dramatically, and the absorption shoulder near 633 nm is lost.[59] Our attempts to measure Raman spectra from high-temperature hematite powder using the 633 nm and 785 nm wavelengths were successful to at most 400 °C and 600 °C. Using the 532 nm laser, we measured Raman signal to a maximum temperature of about 700 °C, but this benchmark increased to over 1050 °C when we replaced the hematite powder with a high-density sample. In this case, the higher packing density allowed for higher light intensities and stronger Raman scattering but is not realistic for CLC applications. In the ultraviolet, a cw 360 nm laser provided

relatively weak Raman signals from room-temperature hematite, but because of the low thermal background, measurable S/N remained when we heated a high-density hematite sample to over 1000 °C (Table 1, Figure 7). Unlike the 532 nm studies, the sample's density did not appreciably impact the S/N in a configuration that included a 40 mm lens for light focusing/collection. Because this UV laser was loaned to us for a limited period by Opto Engine, LLC, full optimization of the setup, including light intensity and collection, was not completed. These preliminary results indicate that a cw wavelength near 360 nm, once optimized, promises some of the strongest potential for Raman measurements from high-temperature hematite powders.

	360 nm	**532 nm**	**633 nm**	**785 nm**
Intensity	$\leq 10^6$ W/cm^2	$\leq 10^5$ W/cm^2	$\leq 10^5$ W/cm^2	$\leq 10^5$ W/cm^2
Highest Temperature	1050 °C	700 °C	400 °C	600 °C

Table 1. A summary of optimized light intensities and maximum achieved temperatures for Raman measurements from hematite powders (600 μm), with the exception of the 360 nm setup, for which the light intensity was not optimized and only estimated, and the sample consisted of densely packed powder.

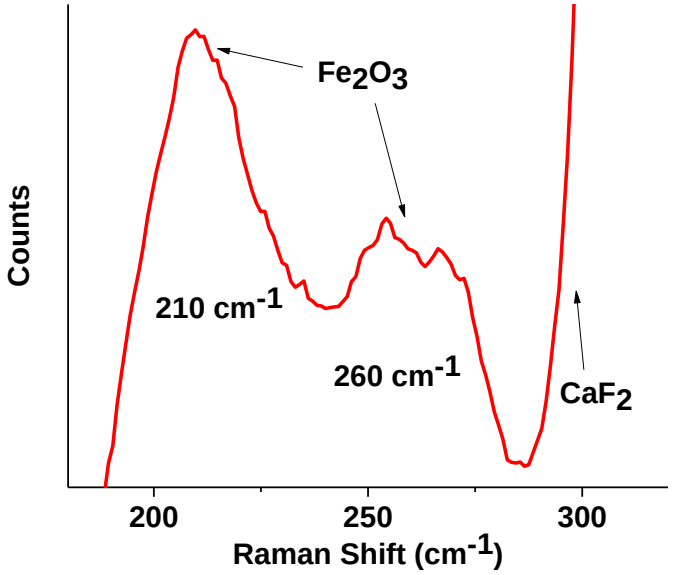

Figure 7. Raman spectrum from Fe_2O_3 at 1000 °C using 360 nm cw light, integrated over 240 s. The raw spectrum has been smoothed using a 21-point, 2nd order Savitzky-Golay filter. The two indicated hematite Raman bands are significantly red-shifted from their normal room temperature values (227 cm^{-1} and 293 cm^{-1}).

Room-temperature measurements from magnetite under ambient conditions can be difficult, because light absorption is very high, easily leading to local temperature increases of hundreds of degrees from a focused laser beam with power of tens of mW,[60] resulting in oxidation to hematite. Our measurements revealed that with a 532 nm laser, 2 mW was sufficient to initiate the oxidation process under ambient conditions, evidenced by formation of maghemite (γ-Fe_2O_3), followed by hematite. When magnetite was evaluated using the other cw wavelengths, only hematite signatures were observed, even at very low powers. In the ultraviolet, further work is needed to test this material within a controlled (inert or reducing) atmosphere.

Raman measurements from high-temperature mixtures of hematite and magnetite

In the above sections, we discussed efforts to optimize Raman signatures from hematite and magnetite in terms of laser (cw/pulsed), light intensity, and wavelength. In this section, we shift our focus to present Raman spectra from high-temperature hematite/magnetite mixtures using currently optimized parameters: cw 532 nm at low light intensity ($\leq 10^5$ W/cm^2). To first provide benchmark data from unmixed, room-temperature powders, we collected Raman spectra from magnetite in an argon environment (Figure 8, black trace) and from hematite in air (Figure 8, red trace). The observed bands are consistent with published values (Table 2), but a few points are noted here: First, in the hematite spectrum, some

laser-induced heating is evident from bands that are red-shifted relative to published values, even when using low-intensity light. Second, a weak hematite band near 659 cm^{-1} can be easily mistaken for magnetite, but the literature provides a convincing argument that this band indeed belongs to hematite, rather than from contamination by magnetite, and is instead a forbidden Raman mode activated by disorder .[61] Third, an intense feature from hematite at 1320 cm^{-1} (not shown) is readily apparent at room temperature, and is likely a second-order overtone of the 660 cm^{-1} band [62]. However, this band disappears above a few hundred degrees Celsius. Finally, an expected, weaker magnetite band at 310 cm^{-1} is at best very faint in the spectrum, while an even weaker feature at 193 cm^{-1} is not always reported and not evident here.

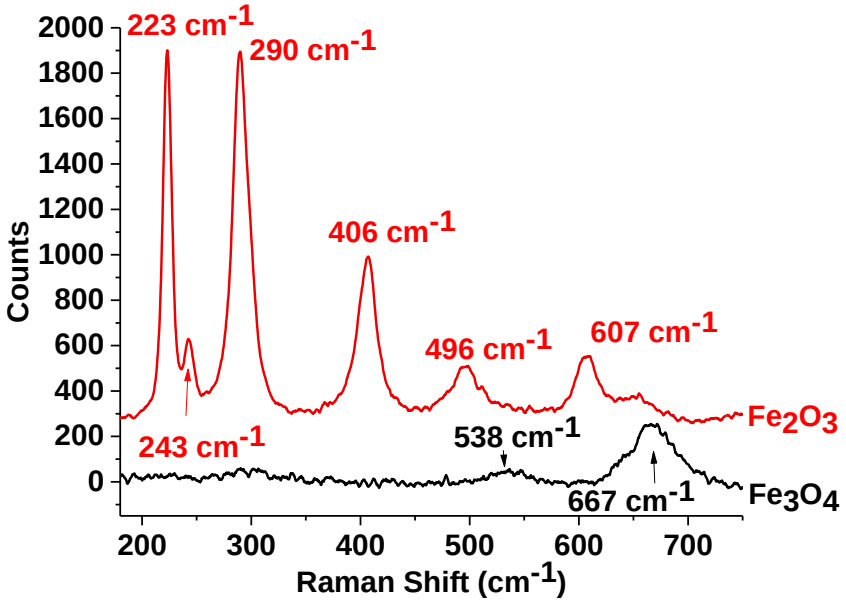

Figure 8. Raman spectra measured from Fe_2O_3 (red) and Fe_3O_4 (black) powders using cw 532 nm at 2 x 10^5 W/cm^2 and 6 x 10^4 W/cm^2, respectively, over 60 s. Data have been background corrected, smoothed, and vertically offset for clarity.

Species	Band center, cm^{-1} (symmetry assignment)
Hematite[61, 62]	226.5 (A_{1g}), 245.5 (E_g), 293.5 (E_g), 300 (E_g), 413 (E_g), 498.5 (A_{1g}), 612.5 (E_g), 659 (E_u), 1320 ($2E_u$)
Magnetite[63]	193 (T_{2g}), 306 (E_g), 538 (T_{2g}), 668 (A_{1g})

Table 2. Band assignments for hematite and magnetite.

In preparation for high-temperature measurements, we combined an equimolar ratio of Fe_2O_3 powder (<212 μm) with Fe_3O_4 powder (3 μm - 70 μm) using a vortex mixer. We placed the powder mixture into the chamber, and then heated it in steps to 600 °C at ~15 °C/min, followed by incremental cooling back to room temperature. Prior to and during the heating/cooling cycle, a high-purity argon source continuously flushed the chamber at 0.8 L/min to minimize oxidation of the sample. The CCD camera collected Raman spectra at each step after the temperature had stabilized, and the spectra are shown in Figures 9 and 10. These figures allow several observations: First, Raman phonon modes expectedly softened and red-shifted with increasing temperature, leading to broader, lower-amplitude bands that can eventually become convoluted with neighboring bands, as well as become difficult to isolate from thermal backgrounds. This is especially true for the magnetite 538 cm^{-1} and 668 cm^{-1} bands, and the hematite 612 cm^{-1} band. These observations were reversible during the cooldown. Second, these spectra indicate that oxidation of the sample occurred during the experiment, evident through a comparison of the relative strength of the hematite and magnetite bands before and after the experiment.

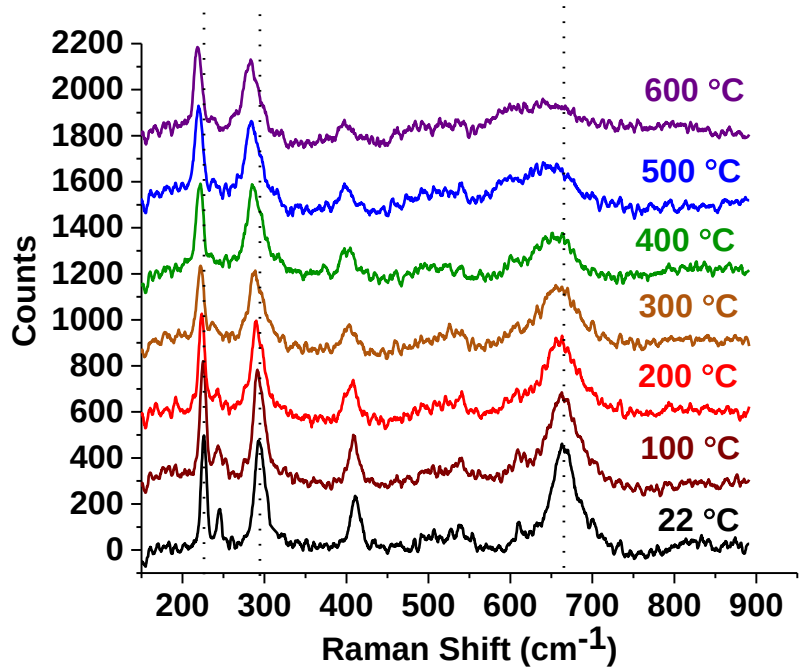

Figure 9. Raman spectra measured from an equimolar Fe_2O_3/Fe_3O_4 mixture while *heating*. Spectra were collected using the cw 532 nm at 3 x 10^4 W/cm^2, with 240 s acquisition. Data have been background corrected, smoothed, and vertically offset for clarity.

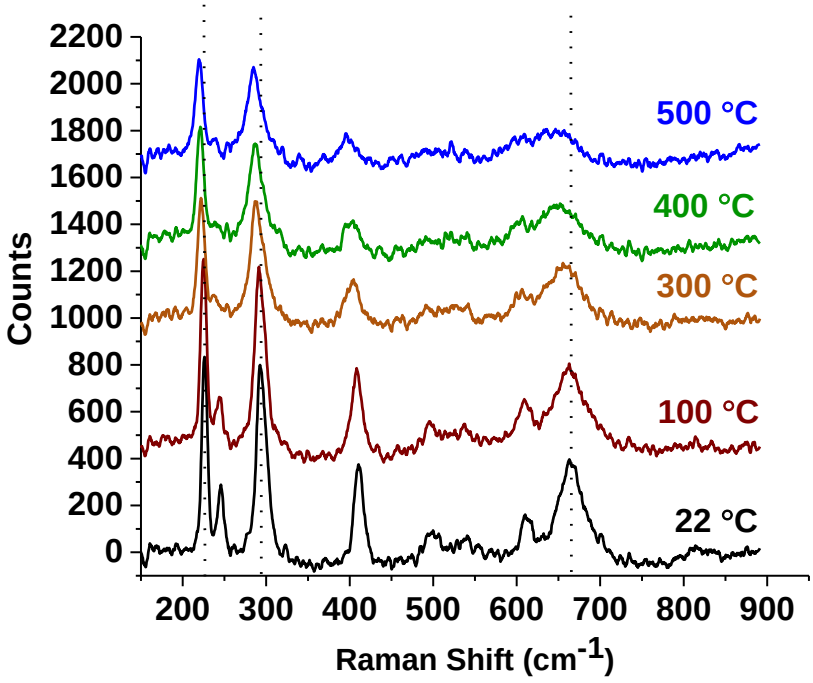

Figure 10. Raman spectra measured from an equimolar Fe_2O_3/Fe_3O_4 mixture while *cooling*. Spectra were collected using the cw 532 nm at 3 x 10^4 W/cm^2, with 240 s acquisition. Data have been background corrected, smoothed, and vertically offset for clarity.

These results highlight some challenges moving forward. First, the magnetite S/N must be increased to ensure detection at temperatures within the CLC operating range (800 °C – 1000 °C). Presently, as these results indicate, the highest

temperature achieved is 600 °C. In a separate experiment that investigated pure Fe_3O_4 powder, the thermal background did not begin to appreciably increase until the temperature crossed 600 °C (Figure 11), corresponding to when magnetite signal was also lost in that experiment. As seen in Figure 9, magnetite S/N decreases with temperature even below 600 °C, and with the addition of thermal radiation declines even further. As mentioned earlier, the best path forward to overcome this challenge will likely include fully optimized, cw excitation in the near-ultraviolet.

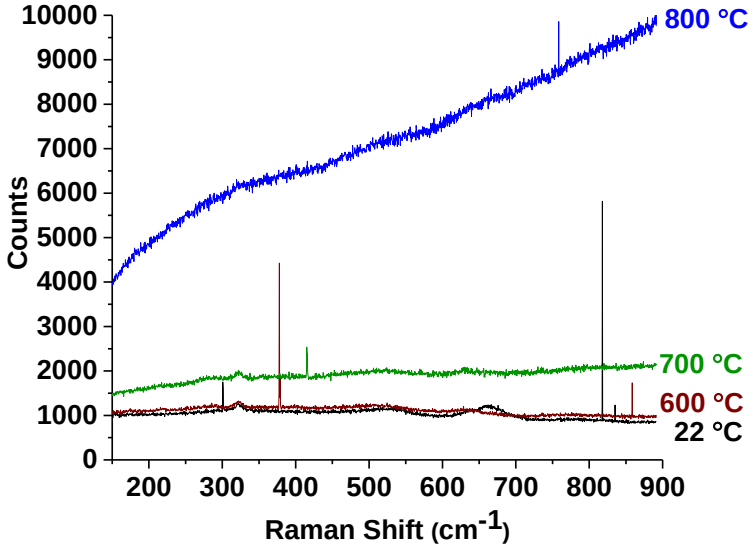

Figure 11. Raw Raman spectra measured from Fe_3O_4 powder at various temperatures. Spectra were collected using cw 532 nm at 6 x 10^4 W/cm^2, with 60 s acquisition.

A second major challenge involves the need to develop a large set of calibration spectra, for which mole fraction and temperature must be well-known, with mole fractions of Fe_2O_3 and Fe_3O_4 ranging from 0% to 100% and temperatures ranging from 700 °C to 1000 °C. Identifying local temperature is not a trivial process, but can be accomplished by assessing Stokes/anti-Stokes intensity ratios [64] or by evaluating band-center shifts against a calibration.[56, 60] Accurately understanding the mole fraction within the laser's probe volume is a larger challenge. The probe volume must be large enough to represent any heterogeneity of the Fe_2O_3/Fe_3O_4 ratio and must represent the mole fraction of the entire sample. This means also that the probe volume must be significantly larger than the largest particle size in the sample. A relatively large probe volume may also eliminate any polarization-dependent signal that could come about when focusing onto a single surface of one grain. A large laser spot size (1 mm – 2 mm) coupled with light collection using a telescope may be one solution to solve this challenge. Another related issue evident from Figures 9 and 10 is the need to "freeze" the oxidation state, or alternatively confirm the local oxidation state *in situ* using an independent method, for calibration purposes. Possibly an integrated, *in situ*, thermogravimetric approach would be feasible but challenging, and is presently beyond the scope of this work. "Freezing" the oxidation state is the more likely approach, but the work presented here indicates that even with high-purity argon (99.9999%), some oxidation of the magnetite sample to hematite occurred when heated to 600 °C. This result is not surprising, given that at 600 °C magnetite is not stable at pO_2 levels above 10^{-6} Pa.[65] Precise control and monitoring of the gas atmosphere, maintained near hematite/magnetite thermodynamic phase boundaries will be critical in a system that likely will include a reducing agent such as hydrogen or methane [66, 67]

Quantifying oxidation states from Raman spectra

Once we have finalized the high-temperature measurement parameters and attained a valid set of calibration data, we will pre-process the spectra and use them to build a multivariate statistical model that relates spectroscopic signatures to mole fraction and temperature. Preprocessing consists of removing cosmic rays, removing thermal backgrounds (both ambient and from laser heating) that can be fitted using a polynomial or measured thermal background, removing all optical artifacts (which are measured and subtracted), and smoothing (typically a 2nd order Savitzky-Golay filter with a 21-point window). We performed these steps in Figures 9 and 10. To fit Raman peaks, Voigt or Gaussian functions typically perform well, and yield three sets of Raman parameters that will be used in the model development: peak position (cm^{-1}), full-width-half-maximum (cm^{-1}), and proportional peak areas. Using an inverse calibration approach outlined by Li et al.[33], a subset of the Raman parameters (R_i) will be related to temperature (T) and mole fraction (x) according to:

$$x = \alpha_o + \alpha_1 R_1 + \alpha_2 R_2 + \ldots + \alpha_h R_h$$

$$T = \beta_o + \beta_1 R_1 + \beta_2 R_{2 + \ldots +} \beta_k R_k$$

In practice, we may implement a slightly modified approach in which a calibration for temperature is first built from data collected from pure materials using the smallest, best-fitting relationship shown above, determined via least-squares analysis. Multiple linear regression (MLR), a common chemometric technique, may be useful for this purpose. Temperature is computed first, because proportional peak areas (and certainly absolute peak areas) will be likely dependent on both T and x, while band centers and likely full width half maximum will depend only on temperature. Several exploratory chemometric techniques, including principle component analysis, should be able to confirm these assertions.

Next, we will relate calibration measurements performed at various temperatures (taken in increments, e.g., every 5 °C – 10 °C) to mole fraction (ranging from 0% - 100%) using the smallest, best-fitting relationship described above. Once again, MLR may be a useful technique for this purpose. As a side point, if instead the proportional peak areas are determined to be independent of temperature, and depend only on mole fraction, data collection and analysis for the calibration model will be greatly simplified, and calibration data from mixtures will only be collected at room temperature, when oxidation states are relatively stable.

As a final note, the procedure described above requires careful curve fitting of pre-processed spectra, which we will first accomplish by hand. However, with automated data processing in view, care must be taken that an algorithm is properly developed that correctly identifies peaks, especially in noisy spectra. This algorithm would likely involve a process that sufficiently smooths the data and looks for a peak maximum within a defined spectral window. (For example, the hematite's low frequency A_g band center varies from about 216 cm^{-1} to 210 cm^{-1} between 700 °C and 1000 °C). The band can be fit, the fit quality evaluated, and then reiterated until a fit improvement is no longer achieved.

4. CONCLUSIONS

In this work, an early evaluation of non-contact, stand-off Raman spectroscopy is performed to determine the relative concentrations of oxidized and reduced forms of OCPs at high temperatures. Operating parameters such as laser type (cw/pulsed), wavelength and intensity are evaluated with respect to the Raman spectra collected from calcium sulfate, hematite, and magnetite at high temperatures. Calcium sulfate provides clear Raman signatures using a pulsed/time gated approach, to temperatures >1000 °C. In contrast, iron oxides are much more difficult to study because of their relatively strong light absorbance and low damage thresholds, requiring low-intensity excitation. Raman spectra from hematite/ magnetite mixtures up to 600 °C are presented, using cw 532 nm excitation. However, results from this work point toward a cw, ultraviolet laser as the most reliable approach to reach higher temperatures, to avoid strong thermal backgrounds. Once experimental parameters are fully optimized, calibration data will need to be collected for which temperature and mole fraction are well-known. The challenges/solutions in meeting these requirements are discussed. Finally, an approach to creating a model that relates Raman spectral parameters with temperature and mole fraction is briefly described, using multivariate statistical analysis and chemometric techniques.

5. ACKNOWLEDGMENTS

J.D.K. would like to thank Benjamin Anderson for helpful discussions and assistance regarding the pulsed Raman measurements. We acknowledge and thank the U.S. DOE/NETL Office of Fossil Energy (DE-FE0027840) for funding this work.

6. REFERENCES

[1] S. W. Luo, L. Zeng, and L. S. Fan, "Chemical Looping Technology: Oxygen Carrier Characteristics," (in English), *Annual Review of Chemical and Biomolecular Engineering, Vol 6*, vol. 6, pp. 53-75, 2015.

[2] B. Moghtaderi, "Review of the Recent Chemical Looping Process Developments for Novel Energy and Fuel Applications," (in English), *Energy & Fuels*, vol. 26, no. 1, pp. 15-40, Jan 2012.

[3] P. Wang, N. Means, D. Shekhawat, D. Berry, and M. Massoudi, "Chemical-Looping Combustion and Gasification of Coals and Oxygen Carrier Development: A Brief Review," (in English), *Energies*, vol. 8, no. 10, pp. 10605-10635, Oct 2015.

[4] L. Liu and M. R. Zachariah, "Enhanced Performance of Alkali Metal Doped Fe_2O_3 and Fe_2O_3/Al_2O_3 Composites As Oxygen Carrier Material in Chemical Looping Combustion," (in English), *Energy & Fuels,* vol. 27, no. 8, pp. 4977-4983, Aug 2013.

[5] W. Liu, J. S. Dennis, and S. A. Scott, "The Effect of Addition of ZrO_2 to Fe_2O_3 for Hydrogen Production by Chemical Looping," (in English), *Industrial & Engineering Chemistry Research,* vol. 51, no. 51, pp. 16597-16609, Dec 26 2012.

[6] Y. Z. Liu, W. H. Jia, Q. J. Guo, and H. J. Ryu, "Effect of Gasifying Medium on the Coal Chemical Looping Gasification with $CaSO_4$ as Oxygen Carrier," (in English), *Chinese Journal of Chemical Engineering,* vol. 22, no. 11-12, pp. 1208-1214, Nov 2014.

[7] Z. S. Liu, Y. G. Wei, K. Z. Li, H. Wang, X. Zhu, and Y. P. Du, "The preparation methods of Fe_2O_3/Al_2O_3 oxygen carriers and their chemical looping combustion performance," (in English), *Applied Energy Technology, Pts 1 and 2,* vol. 724-725, pp. 1145-1149, 2013.

[8] A. Lyngfelt, "Oxygen Carriers for Chemical Looping Combustion-4000 h of Operational Experience," (in English), *Oil & Gas Science and Technology-Revue D Ifp Energies Nouvelles,* vol. 66, no. 2, pp. 161-172, Mar-Apr 2011.

[9] M. Ryden, E. Cleverstam, M. Johansson, A. Lyngfelt, and T. Mattisson, "Fe_2O_3 on Ce-, Ca-, or Mg-Stabilized ZrO_2 as Oxygen Carrier for Chemical-Looping Combustion Using NiO as Additive," (in English), *Aiche Journal,* vol. 56, no. 8, pp. 2211-2220, Aug 2010.

[10] M. Ryden, D. Z. Jing, M. Kallen, H. Leion, A. Lyngfelt, and T. Mattisson, "CuO-Based Oxygen-Carrier Particles for Chemical-Looping with Oxygen Uncoupling - Experiments in Batch Reactor and in Continuous Operation," (in English), *Industrial & Engineering Chemistry Research,* vol. 53, no. 15, pp. 6255-6267, Apr 16 2014.

[11] M. Ryden, M. Johansson, E. Cleverstam, A. Lyngfelt, and T. Mattisson, "Ilmenite with addition of NiO as oxygen carrier for chemical-looping combustion," (in English), *Fuel,* vol. 89, no. 11, pp. 3523-3533, Nov 2010.

[12] M. Ryden, M. Johansson, A. Lyngfelt, and T. Mattisson, "NiO supported on Mg-ZrO_2 as oxygen carrier for chemical-looping combustion and chemical-looping reforming," (in English), *Energy & Environmental Science,* vol. 2, no. 9, pp. 970-981, 2009.

[13] M. Ryden, M. Kallen, D. Z. Jing, A. Hedayati, T. Mattisson, and A. Lyngfelt, "$(Fe_{1-x}Mn_x)Ti_yO_3$ based oxygen carriers for chemical-looping combustion and chemical-looping with oxygen uncoupling," (in English), *7th Trondheim Conference on Co2 Capture, Transport and Storage (2013),* vol. 51, pp. 85-98, 2014.

[14] M. Ryden, A. Lyngfelt, and T. Mattisson, "$CaMn_{0.875}Ti_{0.125}O_3$ as oxygen carrier for chemical-looping combustion with oxygen uncoupling (CLOU)-Experiments in a continuously operating fluidized-bed reactor system," (in English), *International Journal of Greenhouse Gas Control,* vol. 5, no. 2, pp. 356-366, Mar 2011.

[15] M. Ryden, A. Lyngfelt, and T. Mattisson, "Combined manganese/iron oxides as oxygen carrier for chemical looping combustion with oxygen uncoupling (CLOU) in a circulating fluidized bed reactor system," (in English), *10th International Conference on Greenhouse Gas Control Technologies,* vol. 4, pp. 341-348, 2011.

[16] M. Ryden, A. Lyngfelt, T. Mattisson, D. Chen, A. Holmen, and E. Bjorgum, "Novel oxygen-carrier materials for chemical-looping combustion and chemical-looping reforming; $LaxSr_{1-x}Fe_yCo_{1-y}O_3$-delta perovskites and mixed-metal oxides of NiO, Fe_2O_3 and Mn_3O_4," (in English), *International Journal of Greenhouse Gas Control,* vol. 2, no. 1, pp. 21-36, Jan 2008.

[17] M. Ryden, P. Moldenhauer, S. Lindqvist, T. Mattisson, and A. Lyngfelt, "Measuring attrition resistance of oxygen carrier particles for chemical looping combustion with a customized jet cup," (in English), *Powder Technology,* vol. 256, pp. 75-86, Apr 2014.

[18] A. Shafiefarhood, A. Stewart, and F. X. Li, "Iron-containing mixed-oxide composites as oxygen carriers for Chemical Looping with Oxygen Uncoupling (CLOU)," (in English), *Fuel*, vol. 139, pp. 1-10, Jan 1 2015.
[19] K. Shah, B. Moghtaderi, and T. Wall, "Selection of Suitable Oxygen Carriers for Chemical Looping Air Separation: A Thermodynamic Approach," (in English), *Energy & Fuels*, vol. 26, no. 4, pp. 2038-2045, Apr 2012.
[20] A. Shulman, E. Cleverstam, T. Mattisson, and A. Lyngfelt, "Manganese/Iron, Manganese/Nickel, and Manganese/Silicon Oxides Used in Chemical-Looping With Oxygen Uncoupling (CLOU) for Combustion of Methane," (in English), *Energy & Fuels*, vol. 23, pp. 5269-5275, Oct 2009.
[21] L. Silvester, A. Antzara, G. Boskovic, E. Heracleous, A. A. Lemonidou, and D. B. Bukur, "NiO supported on Al_2O_3 and ZrO_2 oxygen carriers for chemical looping steam methane reforming," (in English), *International Journal of Hydrogen Energy*, vol. 40, no. 24, pp. 7490-7501, Jun 29 2015.
[22] H. Song, K. Shah, E. Doroodchi, and B. Moghtaderi, "Development of a Cu-Mg-Based Oxygen Carrier with SiO_2 as a Support for Chemical Looping Air Separation," (in English), *Energy & Fuels*, vol. 28, no. 1, pp. 163-172, Jan 2014.
[23] H. Song, K. Shah, E. Doroodchi, T. Wall, and B. Moghtaderi, "Reactivity of Al_2O_3- or SiO_2-Supported Cu-, Mn-, and Co-Based Oxygen Carriers for Chemical Looping Air Separation," (in English), *Energy & Fuels*, vol. 28, no. 2, pp. 1284-1294, Feb 2014.
[24] Q. L. Song, R. Xiao, Z. Y. Deng, L. H. Shen, and M. Y. Zhang, "Reactivity of a $CaSO_4$-oxygen carrier in chemical-looping combustion of methane in a fixed bed reactor," (in English), *Korean Journal of Chemical Engineering*, vol. 26, no. 2, pp. 592-602, Mar 2009.
[25] Q. L. Song *et al.*, "Chemical-looping combustion of methane with $CaSO_4$ oxygen carrier in a fixed bed reactor," (in English), *Energy Conversion and Management*, vol. 49, no. 11, pp. 3178-3187, Nov 2008.
[26] T. Song, L. H. Shen, S. W. Zhang, D. Q. Chen, and J. Xiao, "Performance of Hematite/$Ca_2Al_2SiO_7$ Oxygen Carrier in Chemical Looping Combustion of Coal," (in English), *Industrial & Engineering Chemistry Research*, vol. 52, no. 22, pp. 7350-7361, Jun 5 2013.
[27] Y. W. Song, J. B. Lee, C. S. Park, G. J. Hwang, H. S. Yang, and Y. H. Kim, "Synthesis and redox properties of NiO/$NiAl_2O_4$ oxygen carriers for hydrogen-fueled chemical-looping combustion," (in English), *Journal of Industrial and Engineering Chemistry*, vol. 12, no. 2, pp. 255-260, Mar 2006.
[28] *Oxy(gen) combustion and Chemical Looping Combustion*. Available: http://www.portalsatc.com/site/conteudo/cursos/carbono/apresentacoes/off/25.pdf
[29] D. M. Chipara, A. C. Chipara, and M. Chipara, "Raman Spectroscopy of Carbonaceous Materials: A Concise Review," (in English), *Spectroscopy*, vol. 26, no. 10, pp. 42-47, Oct 2011.
[30] W. Demtroder, *Laser Spectroscopy*, Fourth ed. Berlin: Springer, 2008.
[31] E. V. Efremov, F. Ariese, and C. Gooijer, "Achievements in resonance Raman spectroscopy review of a technique with a distinct analytical chemistry potential," (in English), *Analytica Chimica Acta*, vol. 606, no. 2, pp. 119-134, Jan 14 2008.
[32] G. Fevotte, "In situ raman spectroscopy for in-line control of pharmaceutical crystallization and solids elaboration processes: A review," (in English), *Chemical Engineering Research & Design*, vol. 85, no. A7, pp. 906-920, Jul 2007.
[33] (1998). *PNNL-12037, Feasibility Study of Using High-Temperature Raman Spectroscopy for On-Line Monitoring and Product Control of the Glass Vitrification Process*.
[34] L. Li, G. S. Hu, J. Q. Lu, and M. F. Luo, "Review of Oxygen Vacancies in CeO_2-Doped Solid Solutions as Characterized by Raman Spectroscopy," (in Chinese), *Acta Physico-Chimica Sinica*, vol. 28, no. 5, pp. 1012-1020, May 2012.
[35] S. Potgieter-Vermaak, N. Maledi, N. Wagner, J. H. P. Van Heerden, R. Van Grieken, and J. H. Potgieter, "Raman spectroscopy for the analysis of coal: a review," (in English), *Journal of Raman Spectroscopy*, vol. 42, no. 2, pp. 123-129, Feb 2011.

[36] W. Qiu and Y. L. Kang, "Mechanical behavior study of microdevice and nanomaterials by Raman spectroscopy: a review," (in English), *Chinese Science Bulletin*, vol. 59, no. 23, pp. 2811-2824, Aug 2014.

[37] R. Thomas and P. Davidson, "Progress in the determination of water in glasses and melt inclusions with Raman spectroscopy: A short review," (in English), *Acta Petrologica Sinica*, vol. 23, no. 1, pp. 15-20, Jan 2007.

[38] D. Wei, S. Chen, and Q. Liu, "Review of Fluorescence Suppression Techniques in Raman Spectroscopy," (in English), *Applied Spectroscopy Reviews*, vol. 50, no. 5, pp. 387-406, 2015.

[39] A. K. Yadav and P. Singh, "A review of the structures of oxide glasses by Raman spectroscopy," (in English), *Rsc Advances*, vol. 5, no. 83, pp. 67583-67609, 2015.

[40] (17 Feb 2016). *Raman Spectroscopy - A Tutorial*. Available: http://www.kosi.com/na_en/products/raman-spectroscopy/raman-technical-resources/raman-tutorial.php

[41] (18 Feb 2016). *Theory of Raman Scattering*. Available: http://bwtek.com/raman-theory-of-raman-scattering/

[42] I. Chourpa *et al.*, "Molecular composition of iron oxide nanoparticles, precursors for magnetic drug targeting, as characterized by confocal Raman microspectroscopy," (in English), *Analyst*, vol. 130, no. 10, pp. 1395-1403, 2005.

[43] R. V. Morris, H. V. Lauer, C. A. Lawson, E. K. Gibson, G. A. Nace, and C. Stewart, "Spectral and Other Physicochemical Properties of Submicron Powders of Hematite (Alpha-Fe_2o_3), Maghemite (Gamma-Fe_2o_3), Magnetite (Fe_3o_4), Goethite (Alpha-FeOOH), and Lepidocrocite (Gamma-FeOOH)," (in English), *Journal of Geophysical Research-Solid Earth and Planets*, vol. 90, no. Nb4, pp. 3126-3144, 1985.

[44] L. Debbichi, M. C. M. de Lucas, J. F. Pierson, and P. Kruger, "Vibrational Properties of CuO and Cu_4O_3 from First-Principles Calculations, and Raman and Infrared Spectroscopy," (in English), *Journal of Physical Chemistry C*, vol. 116, no. 18, pp. 10232-10237, May 10 2012.

[45] R. L. Frost and E. C. Keeffe, "Raman spectroscopic study of the sulfite-bearing minerals scotlandite, hannebachite and orschallite: implications for the desulfation of soils," (in English), *Journal of Raman Spectroscopy*, vol. 40, no. 3, pp. 244-248, Mar 2009.

[46] P. Peikertova, M. Vaculik, P. Filip, and J. Kukutschova, "Raman Microspectroscopy as a Tool for Characterization of Brake Wear Debris," (in English), *Nanocon 2012, 4th International Conference*, pp. 842-846, 2012.

[47] X. Zhang, Y. G. Niu, X. D. Meng, Y. Li, and J. P. Zhao, "Structural evolution and characteristics of the phase transformations between alpha-Fe_2O_3, Fe_3O_4 and gamma-Fe_2O_3 nanoparticles under reducing and oxidizing atmospheres," (in English), *Crystengcomm*, vol. 15, no. 40, pp. 8166-8172, 2013.

[48] B. O. Mysen and J. D. Frantz, "Structure of Silicate Melts at High-Temperature - in-Situ Measurements in the System BaO-SiO_2 to 1669 ^oC," (in English), *American Mineralogist*, vol. 78, no. 7-8, pp. 699-709, Jul-Aug 1993.

[49] T. D. Chaplin, N. L. Ross, and B. Reynard, "A high-temperature and high-pressure Raman spectroscopic study of $CaGeO_3$ garnet," (in English), *Physics and Chemistry of Minerals*, vol. 27, no. 3, pp. 213-219, Feb 2000.

[50] H. F. Garces, B. S. Senturk, and N. P. Padture, "In situ Raman spectroscopy studies of high-temperature degradation of thermal barrier coatings by molten silicate deposits," (in English), *Scripta Materialia*, vol. 76, pp. 29-32, Apr 2014.

[51] S. V. Goryainov, A. S. Krylov, A. N. Vtyurin, and Y. M. Pan, "Raman study of datolite $CaBSiO_4(OH)$ at simultaneously high pressure and high temperature," (in English), *Journal of Raman Spectroscopy*, vol. 46, no. 1, pp. 177-181, Jan 2015.

[52] R. Le Parc *et al.*, "In situ high pressure and high temperature Raman studies of (1-x)SiO_2xGeO_2 glasses," (in English), *Journal of Physics-Condensed Matter*, vol. 21, no. 37, Sep 16 2009.

[53] W. S. Song, G. X. Y. Huang, R. C. Dai, Z. P. Wang, and Z. M. Zhang, "Raman scattering and photoluminescence investigation of YBO_3:Eu^{3+} under high temperature and high pressure," (in English), *Journal of Materials Chemistry C,* vol. 3, no. 10, pp. 2405-2412, 2015.

[54] G. F. Piepel, H. Li, C. F. Windisch, Y. Su, and M. L. Elliott, "Statistical Modeling of Raman Spectroscopy data from high-temperature glass melts for on-line monitoring of temperature and composition," *Quality Engineering,* vol. 13, no. 4, pp. 667-677, 2001.

[55] X. Z. Yang, L. Dubrovinsky, M. A. G. M. Manthilake, and Q. G. Wei, "High-pressure and high-temperature Raman spectroscopic study of hydrous wadsleyite (beta-Mg_2SiO_4)," (in English), *Physics and Chemistry of Minerals,* vol. 39, no. 1, pp. 57-64, Jan 2012.

[56] J. Kirtley, V. Leichner, B. R. Anderson, and H. Eilers, "A Comparison of Pulsed and Continuous Lasers for High-Temperature Raman Measurements of Anhydrite," *Journal of Raman Spectroscopy,* pp. 1-10, 2018.

[57] S. K. Sharma, A. K. Misra, P. G. Lucey, and R. C. F. Lentz, "A combined remote Raman and LIBS instrument for characterizing minerals with 532 nm laser excitation," *Spectrochimica Acta Part a-Molecular and Biomolecular Spectroscopy,* vol. 73, no. 3, pp. 468-476, Aug 2009.

[58] M. K. Nieuwoudt, J. D. Comins, and I. Cukrowski, "The growth of the passive film on iron in 0.05 M NaOH studied in situ by Raman micro-spectroscopy and electrochemical polarisation. Part I: near-resonance enhancement of the Raman spectra of iron oxide and oxyhydroxide compounds," (in English), *Journal of Raman Spectroscopy,* Article vol. 42, no. 6, pp. 1335-1339, Jun 2011.

[59] Y. Yamanoi, S. Nakashima, and M. Katsura, "Temperature dependence of reflectance spectra and color values of hematite by in situ, high-temperature visible micro-spectroscopy," *American Mineralogist,* vol. 94, no. 1, pp. 90-97, Jan 2009.

[60] O. N. Shebanova and P. Lazor, "Raman study of magnetite (Fe3O4): laser-induced thermal effects and oxidation," (in English), *Journal of Raman Spectroscopy,* Article vol. 34, no. 11, pp. 845-852, Nov 2003.

[61] D. Bersani, P. P. Lottici, and A. Montenero, "Micro-Raman investigation of iron oxide films and powders produced by sol-gel syntheses," (in English), *Journal of Raman Spectroscopy,* Article vol. 30, no. 5, pp. 355-360, May 1999.

[62] S. H. Shim and T. S. Duffy, "Raman spectroscopy of Fe2O3 to 62 GPa," (in English), *American Mineralogist,* Article vol. 87, no. 2-3, pp. 318-326, Feb-Mar 2002.

[63] O. N. Shebanova and P. Lazor, "Raman spectroscopic study of magnetite (FeFe2O4): a new assignment for the vibrational spectrum," (in English), *Journal of Solid State Chemistry,* Article vol. 174, no. 2, pp. 424-430, Sep 2003.

[64] G. I. Pangilinan and Y. M. Gupta, "Use of time-resolved Raman scattering to determine temperatures in shocked carbon tetrachloride," (in English), *Journal of Applied Physics,* Article vol. 81, no. 10, pp. 6662-6669, May 1997.

[65] G. Ketteler, W. Weiss, W. Ranke, and R. Schlogl, "Bulk and surface phases of iron oxides in an oxygen and water atmosphere at low pressure," (in English), *Physical Chemistry Chemical Physics,* Article vol. 3, no. 6, pp. 1114-1122, 2001.

[66] J. Zielinski, I. Zglinicka, L. Znak, and Z. Kaszkur, "Reduction of Fe2O3 with hydrogen," (in English), *Applied Catalysis a-General,* Article vol. 381, no. 1-2, pp. 191-196, Jun 2010.

[67] Y. X. Zhang, E. Doroodchi, and B. Moghtaderi, "Reduction Kinetics of Fe2O3/Al2O3 by Ultralow Concentration Methane under Conditions Pertinent to Chemical Looping Combustion," (in English), *Energy & Fuels,* Article vol. 29, no. 1, pp. 337-345, Jan 2015.